Michigan State University

National Superconducting Cyclotron Laboratory

RADIAL FLOW in $^{40}Ar + ^{45}Sc$ at E = (35 - 115) MeV/nucleon

R. PAK, D. CRAIG, E.E. GUALTIERI, S.A. HANNUSCHKE, R.A. LACEY, J. LAURET, W.J. LLOPE, N.T.B. STONE, A.M. VANDER MOLEN, G.D. WESTFALL, and J. YEE

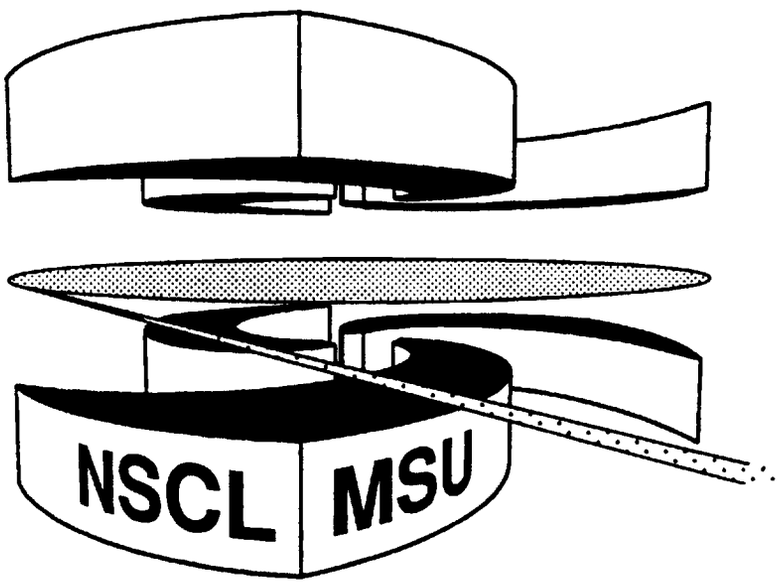

MSUCL-1017 **MARCH 1996**

Radial Flow in ^{40}Ar+^{45}Sc Reactions at E = (35 - 115) MeV/nucleon

R. Pak,[1] D. Craig,[1] E. E. Gualtieri,[1] S. A. Hannuschke,[1] R. A. Lacey,[2] J. Lauret,[2] W. J. Llope,[3] N. T. B. Stone,[1] A. M. Vander Molen,[1] G. D. Westfall,[1] and J. Yee[1]

[1] *National Superconducting Cyclotron Laboratory and Department of Physics and Astronomy, Michigan State University, East Lansing, MI 48824-1321, USA*

[2] *Department of Chemistry, State University of New York at Stony Brook, Stony Brook, NY 11794-3400, USA*

[3] *T.W. Bonner Nuclear Laboratory, Rice University, Houston, TX 77251-1892, USA*

Abstract

Collective radial flow of light fragments from ^{40}Ar+^{45}Sc reactions at beam energies between 35 and 115 MeV/nucleon has been investigated using the Michigan State University 4π Array. The mean transverse kinetic energy $\langle E_t \rangle$ of the different fragment types increases with event centrality, and increases as a function of the incident beam energy. Comparison of our measured values of $\langle E_t \rangle$ shows agreement with predictions of Boltzmann-Uehling-Uhlenbeck (BUU) model and WIX multifragmentation model calculations. The radial flow extracted from $\langle E_t \rangle$ accounts for approximately half of the emitted particle's energy for the heavier fragments ($Z \geq 4$) at the highest beam energy studied.

PACS Number: 25.70.Pq

[illegible] MeV/nucleon, for fragments with Z = 1, 3, 12, and 18, respectively.

Collective motion of nucleons in heavy-ion collisions offers a glimpse at the true many-body effects not present in simple superpositions of individual two-body interactions. Derivation of an equation of state (EOS) for nuclear matter has been the main motivation for studying the collective effects resulting from these collisions. Collective radial expansion of particle emission from central nuclear collisions, termed radial flow, was originally postulated to explain the observed differences in the slopes of the inclusive pion and proton energy spectra [1]. Radial flow was primarily attributed to the conversion of thermal and compressional energy into work through a pressure gradient in the hydrodynamic limit [1, 2]. Consequently, the fragments acquire a net outward radial velocity in addition to their random thermal component, which is evident from the increased curvature in the single-particle energy spectrum. After directed collective transverse flow was demonstrated to be a signature of hydrodynamical compression [3], a study of transverse energy production [4] was undertaken, aimed at accounting for the discrepancy between the measured and calculated thermal mean transverse energies. In that investigation, approximately 40% of the total kinetic energy in the center-of-mass (c.m.) frame was reported to be converted into compressional energy in the moment of highest density [4]. Subsequent work [5, 6, 7, 8, 9, 10, 11] for heavy systems at relatively high beam energies ($\geq$ 100 MeV/nucleon) has also revealed that radial flow is a major contribution to the energy dissipation in the disassembly process of excited nuclear matter.

Indications are that radial flow persists down into the intermediate beam energy regime [12, 13, 14, 15, 16, 17, 18, 19], and is also important for spectator emission from the excited projectile-like fragment [8, 19]. This radial flow phenomenon may even lead to the transient

formation of hollow structures such as bubbles or toroids [20] at these projectile energies. We present results from a systematic study for the incident beam energy and impact parameter dependence of collective radial flow for a relatively light system in this energy regime. Comparison to predictions of Boltzmann-Uehling-Uhlenbeck (BUU) model and WIX multifragmentation model calculations showing agreement with our measured values of radial flow observables are presented. We shall show that the relative contribution of collective radial flow extracted from the mean transverse kinetic energy accounts for approximately half of the emitted particle's energy for the heavier fragments ($Z \geq 4$) at the highest beam energy studied here.

The present measurements were carried out with the Michigan State University 4π Array [21] at the National Superconducting Cyclotron Laboratory (NSCL) using beams from the K1200 cyclotron. A target of 1.0 mg/cm^2 Sc was bombarded with ^{40}Ar projectiles ranging in energy between 35 and 115 MeV/nucleon in 10 MeV/nucleon steps. Beam intensities were approximately 100 electrical pA. Prior to this experiment, the MSU 4π Array was upgraded with the High Rate Array (HRA). The HRA is a close-packed pentagonal configuration of 45 phoswich detectors spanning laboratory polar angles $3° \lesssim \theta_{lab} \lesssim 18°$. With the HRA we obtained Z resolution up to the charge of the ^{40}Ar projectile, and mass resolution for the hydrogen isotopes. The array has good granularity, minimum dead area, and high data rate capability. Low energy thresholds for the HRA are approximately 13, 15, 32, and 37 MeV/nucleon, for fragments with $Z = 1$, 3, 12, and 18, respectively.

The main ball of the MSU 4π Array consists of 170 phoswich detectors (arranged in 20 hexagonal and 10 pentagonal subarrays) covering $18° \lesssim \theta_{lab} \lesssim 162°$. The 30 Bragg curve

counters (BCCs) installed in front of the hexagonal and pentagonal subarrays were operated in ion chamber mode with a pressure of 125 Torr of C_2F_6 gas. The hexagonal anodes of the five most forward BCCs are segmented, resulting in a total of 55 separate ΔE detectors (the BCCs served as ΔE detectors for charged particles that stopped in the fast plastic scintillator of the main ball). Consequently, the main ball was capable of detecting charged fragments from $Z = 1$ to $Z = 16$, with mass resolution for the hydrogen isotopes in the phoswiches. Low energy thresholds were approximately 18, 3.5, and 7 MeV/nucleon for fragments with $Z = 1$, 3, and 12, respectively. Data were taken with a minimum bias trigger that required at least one hit in the HRA (HRA-1 data), and a more central trigger where at least two hits in the main ball (Ball-2 data) were required. The radial flow analysis described below was performed with the Ball-2 data.

The importance of selecting central events to search for a radial flow signal has been emphasized [6, 9, 11, 13, 16] because stopping power, compression, and equilibration are expected to be greatest for collisions at small impact parameters. We assign the impact parameter b of each event through cuts on centrality variables [22] measured with the improved acceptance of the upgraded MSU 4π Array. The centrality variable chosen for the present analysis was the midrapidity charge of each event Z_{mr}, as defined in Ref. [23]. Using methods similar to those detailed in Ref. [24], Z_{mr} is found to be an appropriate variable to use as a centrality filter for this system over the range of beam energies studied, and does not autocorrelate with the radial flow observables. Events with larger Z_{mr} correspond to events with smaller impact parameters.

As an example of the method used for impact parameter selection, events with midra-

pidity charge in the top 10% of the impact-parameter-inclusive Z_{mr} spectrum for the Ball-2 data were assigned to the most central bin. This corresponds to a reduced impact parameter of $\hat{b} = (b/b_{max}) \leq 0.32$ as calculated through a simple geometric prescription [22], where b_{max} represents the largest impact parameter leading to a triggered event. Comparison of events from the Ball-2 trigger to those from the less selective HRA-1 trigger imply that $b_{max} = 0.88 \pm 0.04(R_{proj} + R_{targ})$, where $R_{proj} + R_{targ}$ is the sum of the projectile and target radii. This results in a corrected $\hat{b} \leq 0.28$ for the top 10% most central Ball-2 events. Details of this correction method and the remaining reduced impact parameter bins used in the analysis below are given elsewhere [25].

In addition to selecting central collisions to search for a radial flow signal, reaction products should be measured at 90° in the center-of-mass (c.m.) frame to suppress the contamination by spectator emission and directed flow effects [1, 5, 7, 11]. We show in Fig. 1 the effect of placing various centrality and angular gating conditions on the data. The mean transverse kinetic energy $\langle E_t \rangle$ is plotted versus the mass number A for fragments up to carbon from ^{40}Ar+^{45}Sc reactions at a beam energy of 115 MeV/nucleon. The errors shown are statistical. A systematic increase in the values of $\langle E_t \rangle$ for central events without any angular cut (solid squares) is observed for all fragments over the inclusive (open squares) data set. The values of $\langle E_t \rangle$ for these two data types have been multiplied by a factor of three halves for comparison to the data at 90° in the c.m. frame ($\theta_{\rm c.m.} = 90°$) in accord with Ref. [5]. The values of $\langle E_t \rangle$ again show an increase for all fragments over the inclusive values, when only fragments at 90° ± 15° in the c.m. frame with no restriction on impact parameter (open circles) are considered. The azimuthal rings of detectors at laboratory polar

angles corresponding to this range of angles in the c.m. frame were used to construct this gating condition. Finally, the central event set at $90° \pm 15°$ in the c.m. frame (solid circles) systematically shows the largest values for $\langle E_t \rangle$, demonstrating the importance of satisfying both conditions in searching for a radial flow signal. The trends are essentially preserved for the protons, deuterons, and tritons although the differences between data types are not as pronounced due to contributions from pre-equilibrium emission, and because radial flow has been shown to be smaller for lighter particle species [1, 5, 13, 16]. These selection criteria were applied to the data in the analysis described below.

In Fig. 2 we display the dependence of $\langle E_t \rangle$ on the incident beam energy for the different fragment types at two reduced impact parameter bins. The data are for ^{40}Ar+^{45}Sc reactions at $\theta_{\mathrm{c.m.}} = 90° \pm 15°$, and the errors shown are statistical. The reduced impact parameter bins were determined as in Ref. [25] (the values of b/b_{max} correspond to the upper limit of each bin). For the more central events displayed in the lower panel, the values of $\langle E_t \rangle$ show a monotonic increase as the beam energy increases for all particle types, which becomes particularly dramatic for the larger mass fragments. This is in striking contrast to the more peripheral event set shown in the upper panel, for which the values of $\langle E_t \rangle$ exhibit a gradual increase as a function of beam energy regardless of mass. The difference in the values of $\langle E_t \rangle$ at each beam energy in the upper panel between fragment types is attributed to the difference in the low-energy thresholds in the BCCs for the different particle types, and should not be interpreted as a deviation from thermal equilibrium. This difference (an effect also present in the lower panel) can be made to vanish if an artificial common threshold equal to the low-energy threshold in the BCCs for carbon is made in software on the other

particle types. The apparent leveling of $\langle E_t \rangle$ for heavier fragments in central collisions at beam energies below 55 MeV/nucleon is also an artifact of these low-energy thresholds.

At the higher beam energies, where low-energy thresholds have a less significant effect, the dramatic increase in the values of $\langle E_t \rangle$ for the heavier fragments produced in central collisions is linked to larger values of the radial flow energy. This is in contrast to expectations of a purely thermal source for which the different particle types are emitted with the same mean kinetic energy. For comparison we show in the lower panel the predictions of a purely thermal model calculation, the fireball model [26], at each of the projectile energies (asterisks). These calculations were not corrected for detector acceptance effects. The large values of $\langle E_t \rangle$ for the heavy fragments ($Z \geq 4$) in central collisions at the higher beam energy underscore the importance of radial flow in the nuclear disassembly process for these events.

To examine more thoroughly the impact parameter dependence of $\langle E_t \rangle$, we present in Fig. 3 the mean transverse kinetic energy for the different particle types plotted versus the reduced impact parameter at four incident beam energies. Again the data are for ^{40}Ar+^{45}Sc reactions at $\theta_{\rm c.m.} = 90° \pm 15°$ and the errors shown are statistical. The values of $\hat{b} = b/b_{max}$ correspond to the upper limit of each reduced impact parameter bin. Up to a projectile energy of 55 MeV/nucleon the data exhibit a constant value of $\langle E_t \rangle$ for each particle type, while above 55 MeV/nucleon a monotonic rise in the values of $\langle E_t \rangle$ occurs as the impact parameter becomes smaller. The rising value of $\langle E_t \rangle$ with increasing centrality becomes progressively stronger at higher bombarding energies (the heavier fragments are missing in the largest $\hat{b}$ bin, because of the forward focusing effects in fixed target experiments). This result is in qualitative agreement with previous data [4], and BUU model calculations [5]

for light particle emission (p, d, t, and ^{3}He) from collisions for heavier entrance channels at higher beam energies. The authors of those works attributed this phenomenon to collective expansion of a blast of light fragments in central collisions.

To estimate the magnitude of the mean transverse kinetic energy imparted to the fragments in the nuclear disassembly process, we used a BUU model calculation [27]. In this model the nucleons are assumed to interact with a collectively generated mean field, and with each other through two-body collisions which respect the Pauli exclusion principle. Shown in Fig. 4 for central ^{40}Ar+^{45}Sc reactions at four bombarding energies are results for $\langle E_t \rangle$ of the nucleons as a function of time. The calculations were performed at a fixed impact parameter of $b = 0$ for a EOS with compressibility $\kappa = 240$ MeV, and were not corrected for effects due to detector acceptance. The upper (lower) panel shows the mean transverse kinetic energy per nucleon when only particles that move in a medium whose density is less (greater) than one eighth of the normal nuclear density $\rho_0 = 0.168$ fm^{-3} were included in the calculation. For particles in medium with $\rho/\rho_0 < \frac{1}{8}$, we found collisions are no longer sufficiently frequent to allow conversion of thermal and compressional energy into collective radial flow, so that freeze-out has occurred for these nucleons. The dashed line in the lower panel represents the value of two thirds the Fermi energy of the initial configuration of the system before the collision occurs.

The results displayed in Fig. 4 clearly show that in either case the maximum value of $\langle E_t \rangle$ increases as the projectile energy increases. The present calculations are consistent with a scenario [16] in which the maximum density is reached when the colliding nuclei stop completely within each other and the maximum flow energy is attained shortly afterwards.

Figure Captions

Table 1: The incident beam energy, the measured mean transverse kinetic energy, the temperature, the radial expansion velocity, and the relative fraction of the radial flow energy for Be fragments from central ^{40}Ar+^{45}Sc collisions at polar angles $\theta_{\rm c.m.} = 90° \pm 15°$.

Figure 1: Mean transverse kinetic energy from ^{40}Ar+^{45}Sc reactions at 115 MeV/nucleon versus fragment mass number for various centrality and angular gating conditions as defined in the inset and the text. The lines are included to guide the eye.

Figure 2: Mean transverse kinetic energy of fragments from ^{40}Ar+^{45}Sc reactions at polar angles $\theta_{\rm c.m.} = 90° \pm 15°$ versus incident beam energy for two impact parameters bins. Predictions from the fireball model [26] are shown in lower panel (asterisks).

Figure 3: Mean transverse kinetic energy of fragments from ^{40}Ar+^{45}Sc reactions at polar angles $\theta_{\rm c.m.} = 90° \pm 15°$ versus the reduced impact parameter at four incident beam energies.

Figure 4: Mean transverse kinetic energy per nucleon for ^{40}Ar+^{45}Sc reactions at four bombarding energies as a function of time from BUU theory [27]. The calculations are at a fixed impact parameter of $b = 0$ for a medium EOS. The upper (lower) panel shows $\langle E_t \rangle$ when only particles that move in a medium whose density is less (greater) than one eighth of the normal nuclear density are included in the calculation.

from the value of the height of the first peak for each projectile energy shown in the lower panel of Fig. 4. These values, plotted as solid circles in Fig. 5, show good agreement with the data for fragments with $Z \geq 2$. Although our BUU calculations involve only nucleons, we are still able to delineate the approximate limits on the value of $\langle E_t \rangle$ as a function of incident beam energy reasonably well. This lends further support to the interpretation of the disassembly mechanism garnered from the model, as outlined above.

Using our measured values of $\langle E_t \rangle$, we calculated the radial expansion velocity β_{flow} for the heavier fragments at the highest beam energy where the flow signal is the most pronounced. The mean transverse kinetic energy may be written as:

$$\langle E_t \rangle = \frac{2}{3}\langle E_{thermal} \rangle + \langle E_{radial} \rangle = T + \langle E_{radial} \rangle, \tag{1}$$

because cross terms between the collective and the random thermal components vanish on the average [8]. The sum of the initial expansive flow and the Coulomb induced energy can be non-relativistically approximated by [7, 10]:

$$\langle E_{radial} \rangle = E_{flow} + E_{Coulomb} = \frac{3}{5}\left[\frac{1}{2}m_f c^2 \beta_{flow}^2 + \frac{Z_f(Z_S - Z_f)e^2}{R_S}\right], \tag{2}$$

where subscript S refers to the source and f to the fragment type. In this expression, we have assumed $Z_S = 39$ and $R_S = 8$ fm, representing the maximum Coulomb repulsion from the equilibrated compound source. The radial expansion velocities determined in the present calculation are insensitive to the difference in source size with those reported from fragment coalescence [28]. A temperature parameter of $T = 28$ MeV for an incident beam energy of 115 MeV/nucleon was extracted from a single-source Maxwell-Boltzmann (MB) fit to the proton energy spectrum for central collisions at $\theta_{\mathrm{c.m.}} = 90° \pm 15°$. Protons were used to determine

Figure 5: Mean transverse kinetic energy per nucleon of fragments from central ^{40}Ar+^{45}Sc reactions at polar angles $\theta_{\mathrm{c.m.}} = 90° \pm 15°$ versus incident beam energy compared with predictions of BUU model calculations. The lines are included to guide the eye.

Figure 6: Mean transverse kinetic energy of fragments from central ^{40}Ar+^{45}Sc reactions at polar angles $\theta_{\mathrm{c.m.}} = 90° \pm 15°$ versus incident beam energy compared with predictions of WIX model [29] calculations assuming half the available energy is associated with radial flow. The lines are included to guide the eye.

collective radial expansion of light fragment emission in heavy-ion collisions using the statistical multifragmentation model called WIX [29]. The WIX code generated events in which a single source de-excites via explosion and evaporation with this specified collective expansion energy at freeze-out. The calculations included the Coulomb interaction between fragments, and the default parameters were used to characterize the level density, explosion threshold energy, and spacial configuration of the decaying source. The simulated events were analyzed with the same radial flow routine as for the actual data. In Fig. 6 we show a comparison between data and simulation for the excitation functions of the mean transverse kinetic energy for various light fragment types. The open symbols are data from central ^{40}Ar+^{45}Sc reactions at polar angles $\theta_{\rm c.m.} = 90° \pm 15°$ (as in the lower panel of Fig. 2). The solid symbols are the predictions of the WIX multifragmentation model assuming half the available energy of the disassembly process is associated with radial flow. All effects of the experimental acceptance were included in these filtered simulations. The errors shown are statistical, and the dashed lines are included only to guide the eye. Similar trends are present in the filtered simulation of the other particle types not shown for clarity. The agreement between data and simulation in Fig. 6 demonstrates that the measured radial flow is not an artifact of our detector acceptance or analysis method, and substantiates our claim that approximately half of the emitted particle's energy originates from collective radial expansion.

In summary, we have investigated collective radial flow of light fragments from ^{40}Ar+^{45}Sc reactions at beam energies in the range E = (35 - 115) MeV/nucleon using the MSU 4π Array. The mean transverse kinetic energy of the different fragment types increases with event centrality, and increases as a function of the incident beam energy. Comparison of

E_{beam} (AMeV)	$\langle E_t \rangle$ (MeV)	T (MeV)	β_{flow} (v/c)	$E_{flow}/\langle E_t \rangle$ (%)
115	109	28	0.16	61
105	104	26	0.16	61
95	91	25	0.14	56
85	84	23	0.14	55
75	73	21	0.12	51
65	65	20	0.11	46
55	54	17	0.09	41
45	48	14	0.09	42
35	46	12	0.09	41

Table 1:

[6] S.C. Jeong, N. Herrmann, Z.G. Fan, R. Freifelder, A. Gobbi, K.D. Hildenbrand, M. Krämer, J. Randrup, W. Reisdorf, D. Schüll, U. Sodan, K. Teh, J.P. Wessels, D. Pelte, M. Trzaska, T. Wienold, J.P. Alard, V. Amouroux, Z. Basrak, N. Bastid, I.M. Belayev, L. Berger, M. Bini, Th. Blaich, S. Boussange, A. Buta, R. Čaplar, C. Cerruti, N. Cindro, J.P. Coffin, R. Dona, P. Dupieux, J. Erö, P. Fintz, Z. Fodor, L. Fraysse, S. Frolov, Y. Grigorian, G. Guillaume, S. Hölbling, A. Houari, F. Jundt, J. Kecskemeti, P. Koncz, Y. Korchagin, R. Kotte, C. Kuhn, M. Ibnouzahir, I. Legrand, A. Lebedev, C. Maguire, V. Manko, P. Mauerenzig, G. Mgebrishvili, J. Mösner, D. Moisa, G. Montarou, I. Montbel, P. Morel, W. Neubert, A. Olmi, G. Pasquali, M. Petrovici, G. Poggi, F. Rami, V. Ramillien, A. Sadchikov, Z. Seres, B. Sikora, V. Simion, S. Smolyankin, R. Tezkratt, M.A. Vasiliev, P. Wagner, Z. Wilhelmi, D. Wohlfarth, and A.V. Zhilin, Phys. Rev. Lett. **72**, 3468 (1994).

[7] W.C. Hsi, G.J. Kunde, J. Pochodzalla, W.G. Lynch, M.B. Tsang, M.L. Begemann-Blaich, D.R. Bowman, R.J. Charity, F. Cosmo, A. Ferrero, C.K. Gelbke, T. Glasmacher, T. Hofmann, G. Imme, I. Iori, J. Hubele, J. Kempter, P. Kreutz, W.D. Kunze, V. Lindenstruth, M.A. Lisa, U. Lynen, M. Mang, A. Moroni, W.F.J. Müller, M. Neumann, B. Ocker, C.A. Ogilvie, G.F. Peaslee, G. Raciti, F. Rosenberger, H. Sann, R. Scardaoni, A. Schüttauf, C. Schwarz, W. Seidel, V. Serfling, L.G. Sobotka, L. Stuttge, S. Tomasevic, W. Trautmann, A. Tucholski, C. Williams, A. Wörner, and B Zwieglinski, Phys. Rev. Lett. **73**, 3367 (1994).

[8] G.J. Kunde, W.C. Hsi, W.D. Kunze, A. Schüttauf, A. Wörner, M. Begemann-Blaich,

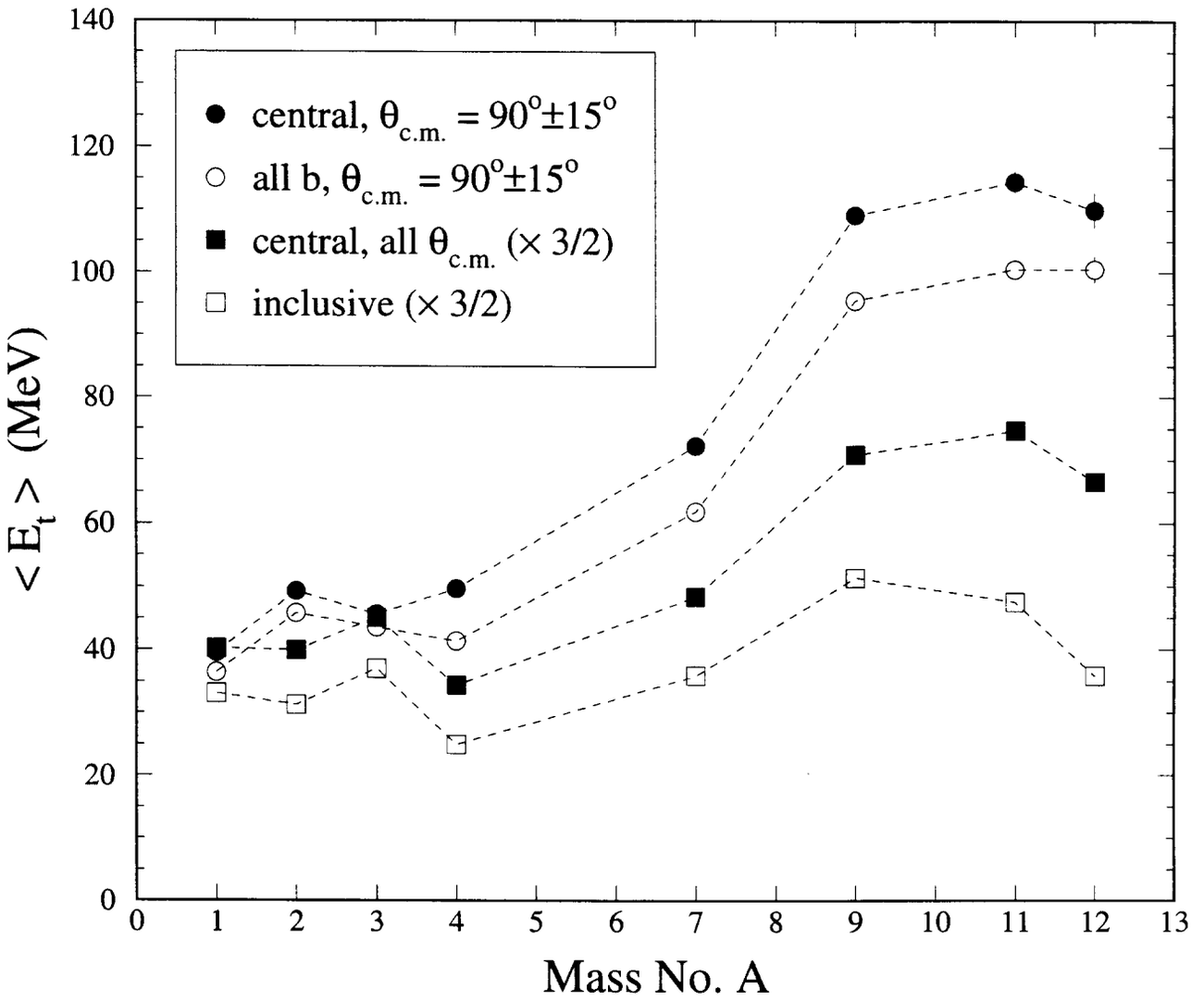
central, $\theta_{c.m.} = 90^{o}\pm15^{o}$
all b, $\theta_{c.m.} = 90^{o}\pm15^{o}$
central, all $\theta_{c.m.}$ (× 3/2)
inclusive (× 3/2)
$< E_t >$ (MeV)
Mass No. A
0
20
40
60
80
100
120
140
0
1
2
3
4
5
6
7
8
9
10
11
12
13

Figure 1:

J.L. Chance, Y. Choi, S. Costa, J.B. Elliot, M.L. Gilkes, J.A. Hauger, A.S. Hirsch, E.L. Hjort, A. Insolia, M. Justice, D. Keane, J. Kintner, H.S. Matis, M. McMahan, C. McParland, D.L. Olson, M.D. Partlan, N.T. Porile, R. Potenza, G. Rai, J. Rasmussen, H.G. Ritter, J. Romanski, J.L. Romero, G.V. Russo, R. Scharenberg, A. Scott, Y. Shao, B.K. Srivastava, T.J.M. Symons, M. Tincknell, C. Tuvé, S. Wang, P. Warren, G.D. Westfall, H.H. Wieman, and K. Wolf, Phys. Rev. Lett. **72**, 2662 (1995).

[12] W.A. Friedman, Phys. Rev. C **42**, 667 (1990).

[13] H.W. Barz, J.P. Bondorf, R. Donangelo, R. Elmér, F.S. Hansen, B. Jakobsson, L. Karlsson, H. Nifenecker, H. Schulz, F. Schussler, K. Sneppen, and K. Söderström, Nucl. Phys. **A531**, 453 (1991).

[14] K. Hagel, M. Gonin, R. Wada, J.B. Natowitz, B.H. Sa, Y. Lou, M. Gui, D. Utley, G. Nebbia, D. Fabris, G. Prete, J. Ruiz, D. Drain, B. Chambon, B. Cheynis, D. Guinet, X.C. Hu, A. Demeyer, C. Pastor, A. Giorni, A. Lleres, P. Stassi, J.B. Viano, and P. Gonthier, Phys. Rev. Lett. **68**, 2141 (1992).

[15] R.T. de Souza, D. Fox, W.A. Friedman, L. Phair, D.R. Bowman, C.K. Gelbke, W.G. Gong, Y.D. Kim, M.A. Lisa, W.G. Lynch, G.F. Peaslee, M.B. Tsang, and F. Zhu, Phys. Lett. B **300**, 29 (1993).

[16] W. Bauer, J.P. Bondorf, R. Donangelo, R. Elmér, B. Jakobsson, H. Schulz, F. Schussler, and K. Sneppen, Phys. Rev. C **47**, R1838 (1993).

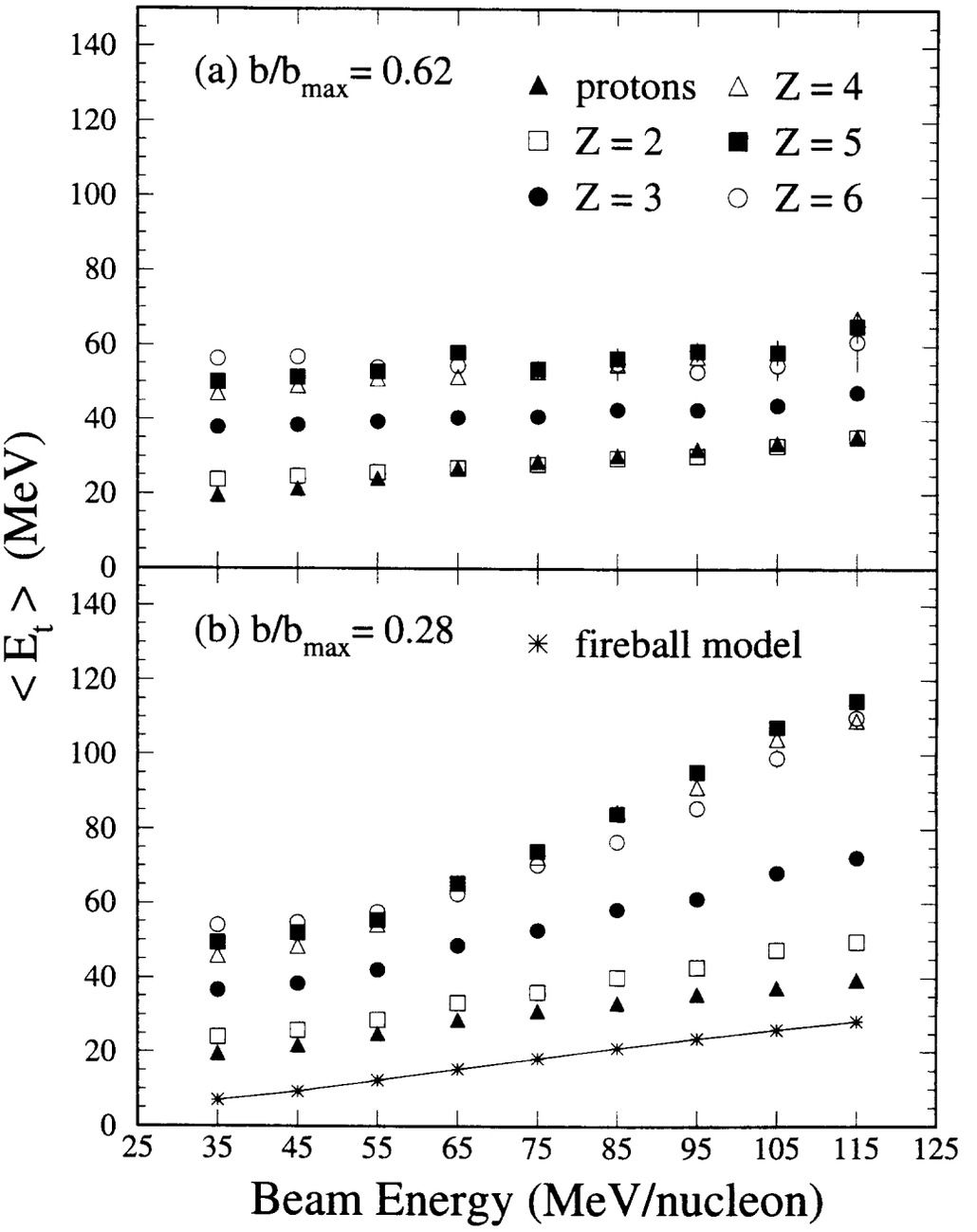
(a) b/b$_{max}$= 0.62
protons
Z = 2
Z = 3
Z = 4
Z = 5
Z = 6
(b) b/b$_{max}$= 0.28
fireball model
< E$_t$ > (MeV)
Beam Energy (MeV/nucleon)
0
20
40
60
80
100
120
140
25
35
45
55
65
75
85
95
105
115
125

Figure 2:

[24] W.J. Llope, J.A. Conrad, C.M. Mader, G. Peilert, W. Bauer, D. Craig, E. Gualtieri, S. Hannuschke, R.A. Lacey, J. Lauret, T. Li, A. Nadasen, E. Norbeck, R. Pak, N.T.B. Stone, A.M. Vander Molen, G.D. Westfall, J. Yee, and S.J. Yennello, Phys. Rev. C **51**, 1325 (1995).

[25] R. Pak, W.J. Llope, D. Craig, E.E. Gualtieri, S.A. Hannuschke, R.A. Lacey, J. Lauret, A.C. Mignerey, D.E. Russ, N.T.B. Stone, A.M. Vander Molen, G.D. Westfall, and J. Yee, Phys. Rev. C (in press).

[26] G.D. Westfall, J. Gosset, P.J. Johansen, A.M. Poskanzer, W.G. Meyer, H.H. Gutbrod, A. Sandoval, and R. Stock, Phys. Rev. Lett. **37**, 1202 (1976).

[27] W. Bauer, G.F. Bertsch, W. Cassing, and U. Mosel, Phys. Rev. C **34**, 2127 (1986); W. Bauer, Phys. Rev. Lett. **61**, 2534 (1988).

[28] W.J. Llope, S.E. Pratt, N. Frazier, R. Pak, D. Craig, E.E. Gualtieri, S.A. Hannuschke, N.T.B. Stone, A.M. Vander Molen, G.D. Westfall, J. Yee, R.A. Lacey, J. Lauret, A.C. Mignerey, and D.E. Russ, Phys. Rev. C **52**, 2004 (1995).

[29] J. Randrup, Comp. Phys. Comm. **77**, 153 (1993).

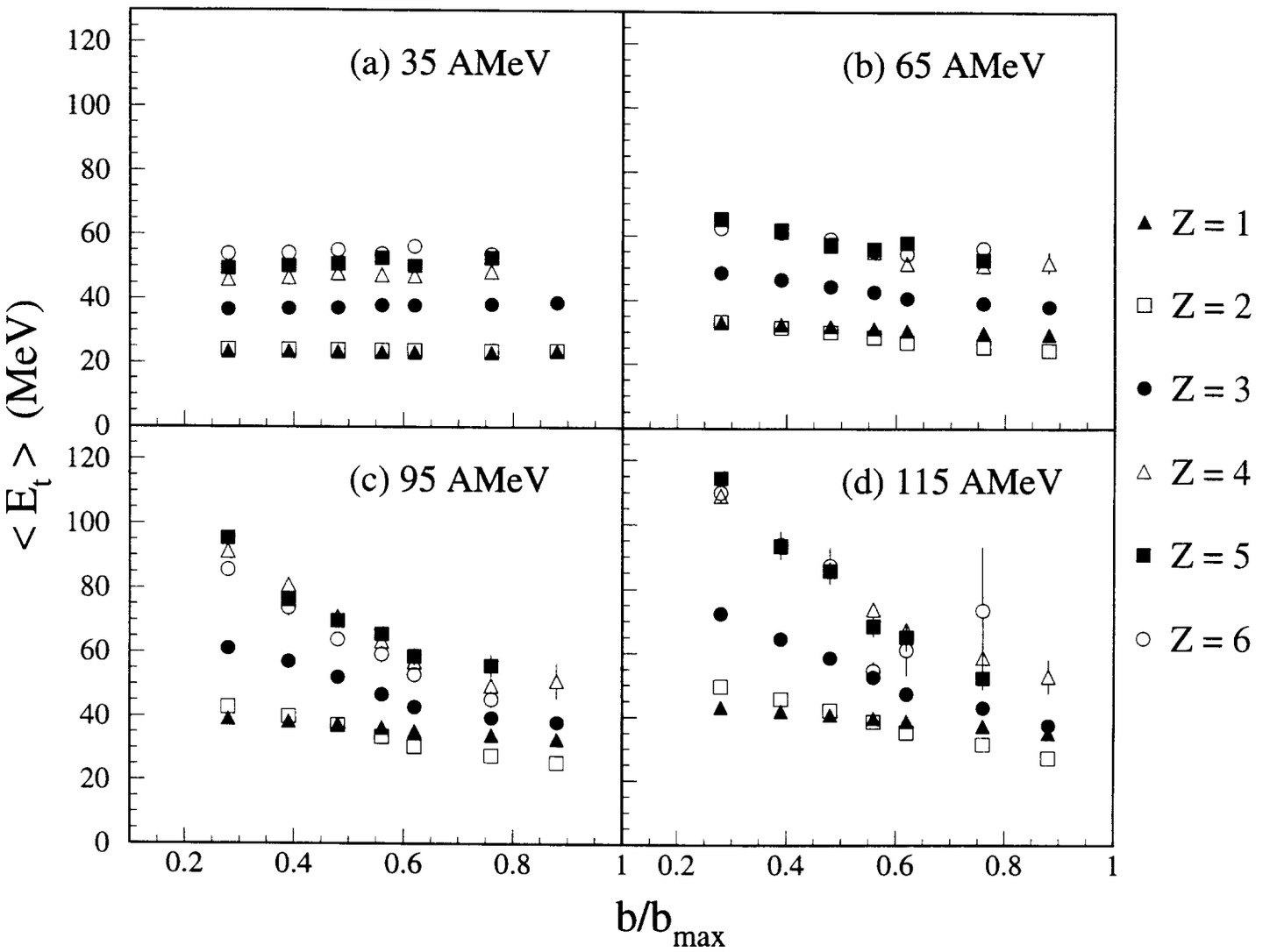
(a) 35 AMeV
(b) 65 AMeV
(c) 95 AMeV
(d) 115 AMeV
< E_t > (MeV)
b/b_max
Z = 1
Z = 2
Z = 3
Z = 4
Z = 5
Z = 6

Figure 3:

Figure 5: Mean transverse kinetic energy per nucleon of fragments from central ^{40}Ar+^{45}Sc reactions at polar angles $\theta_{\mathrm{c.m.}} = 90° \pm 15°$ versus incident beam energy compared with predictions of BUU model calculations. The lines are included to guide the eye.

Figure 6: Mean transverse kinetic energy of fragments from central ^{40}Ar+^{45}Sc reactions at polar angles $\theta_{\mathrm{c.m.}} = 90° \pm 15°$ versus incident beam energy compared with predictions of WIX model [29] calculations assuming half the available energy is associated with radial flow. The lines are included to guide the eye.

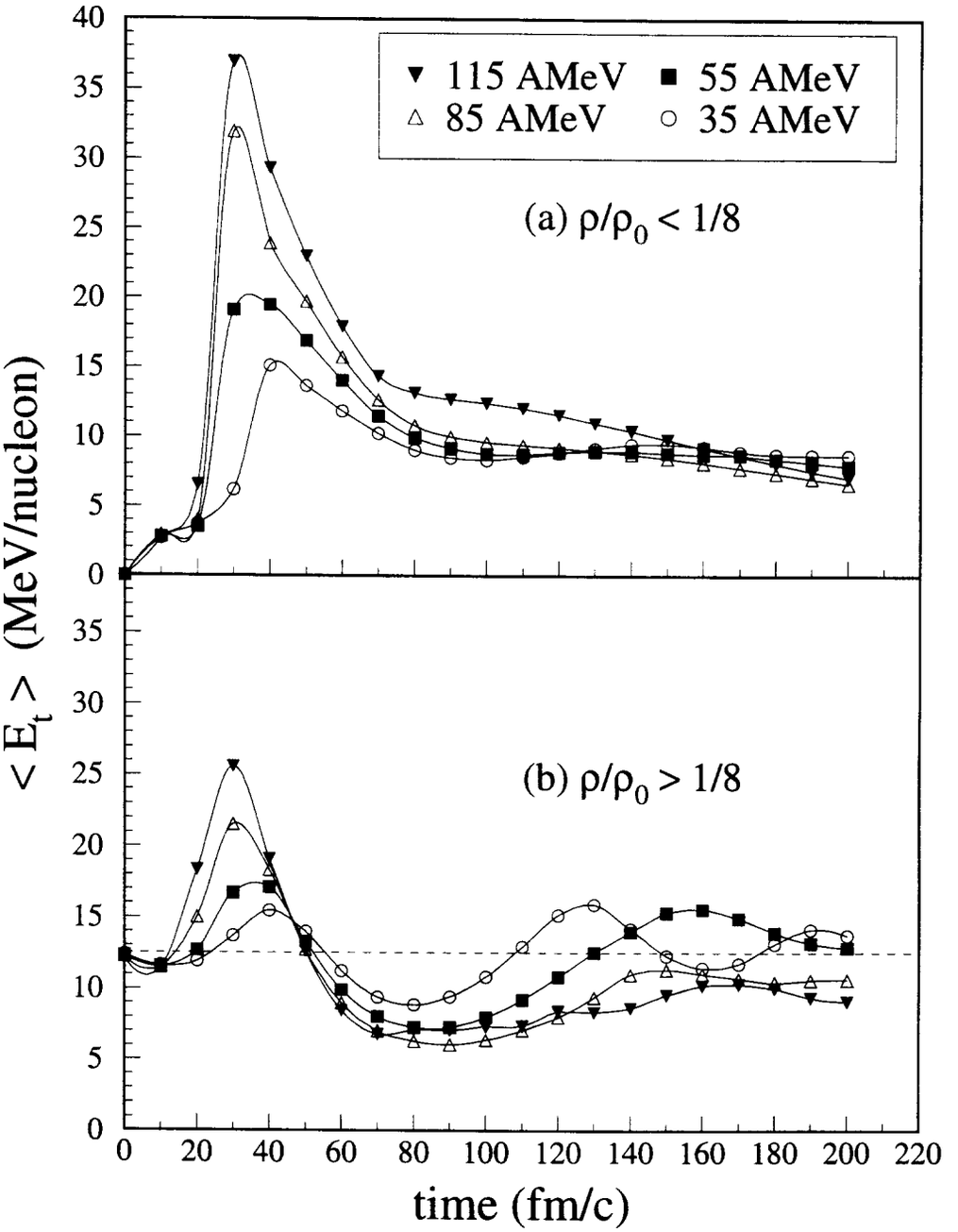
115 AMeV
55 AMeV
85 AMeV
35 AMeV
(a) ρ/ρ0 < 1/8
(b) ρ/ρ0 > 1/8
< Et > (MeV/nucleon)
time (fm/c)
0
5
10
15
20
25
30
35
40
0
20
40
60
80
100
120
140
160
180
200
220

Figure 4:

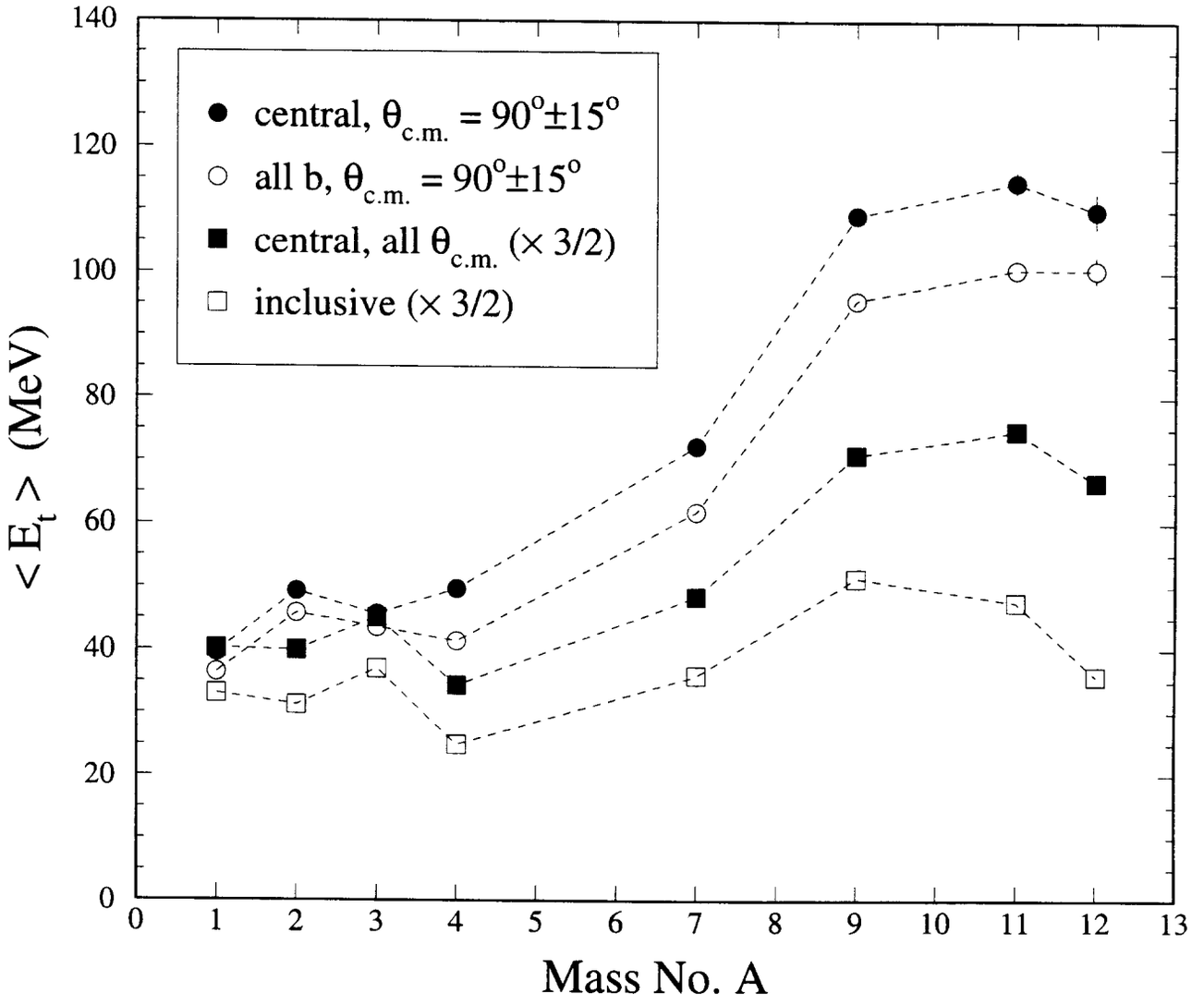
central, $\theta_{c.m.} = 90^{o}\pm15^{o}$
all b, $\theta_{c.m.} = 90^{o}\pm15^{o}$
central, all $\theta_{c.m.}$ ($\times$ 3/2)
inclusive ($\times$ 3/2)
$< E_t >$ (MeV)
Mass No. A
0
20
40
60
80
100
120
140
0
1
2
3
4
5
6
7
8
9
10
11
12
13

Figure 1:

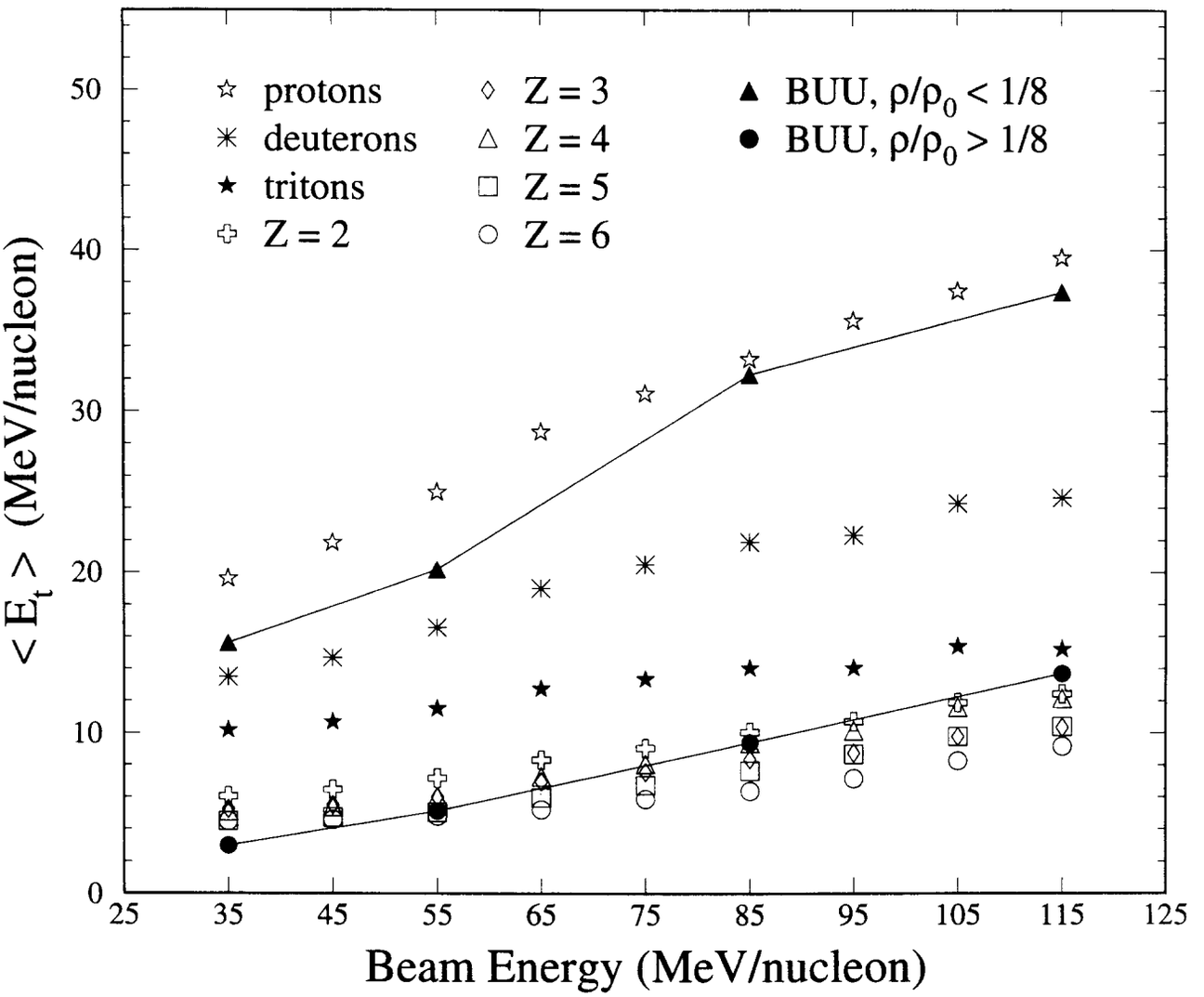
protons
deuterons
tritons
Z = 2
Z = 3
Z = 4
Z = 5
Z = 6
BUU, ρ/ρ0 < 1/8
BUU, ρ/ρ0 > 1/8
< Et > (MeV/nucleon)
Beam Energy (MeV/nucleon)
0
10
20
30
40
50
25
35
45
55
65
75
85
95
105
115
125

Figure 5:

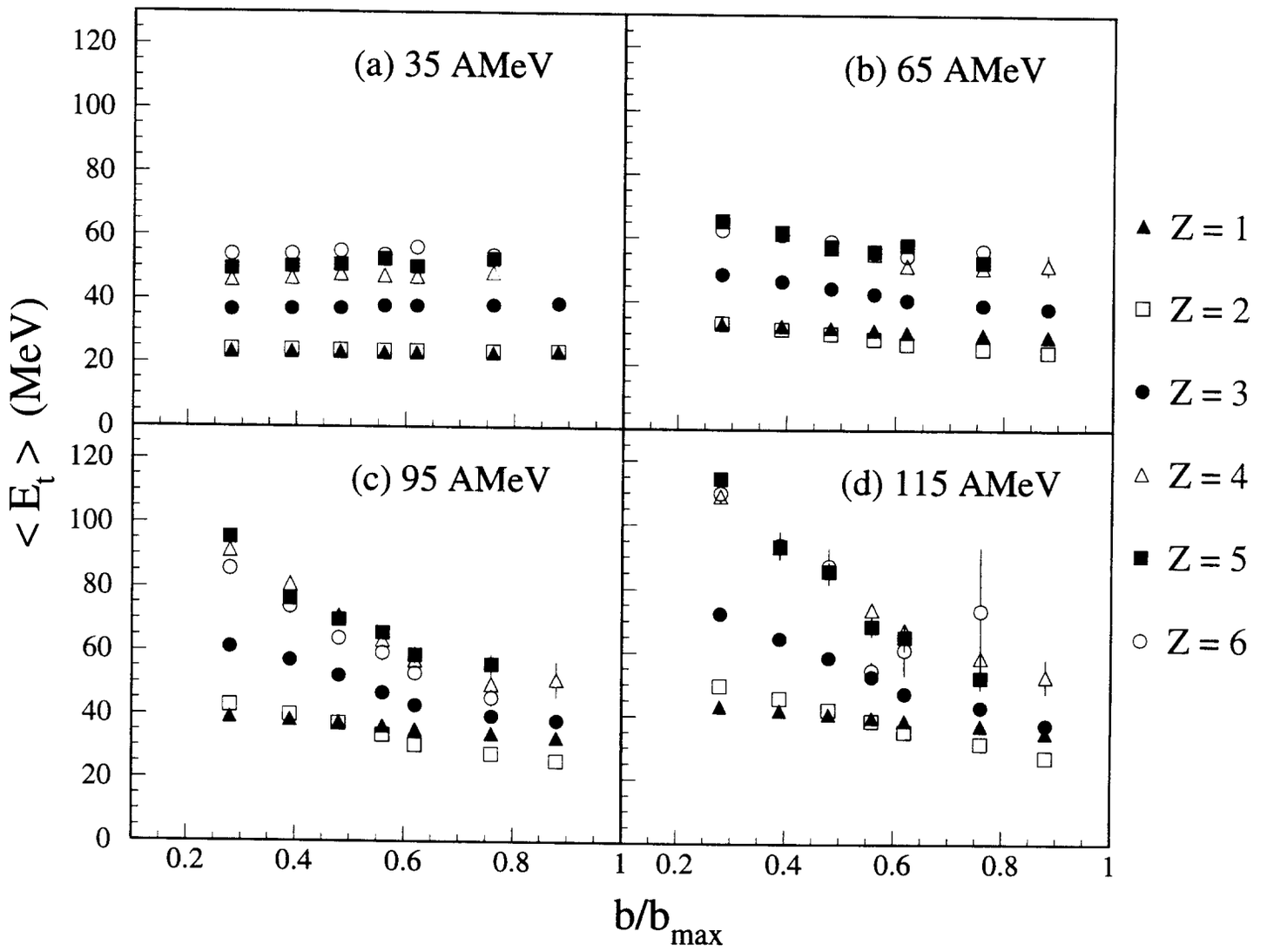
(a) 35 AMeV
(b) 65 AMeV
(c) 95 AMeV
(d) 115 AMeV
< E_t > (MeV)
b/b_max
Z = 1
Z = 2
Z = 3
Z = 4
Z = 5
Z = 6

Figure 3:

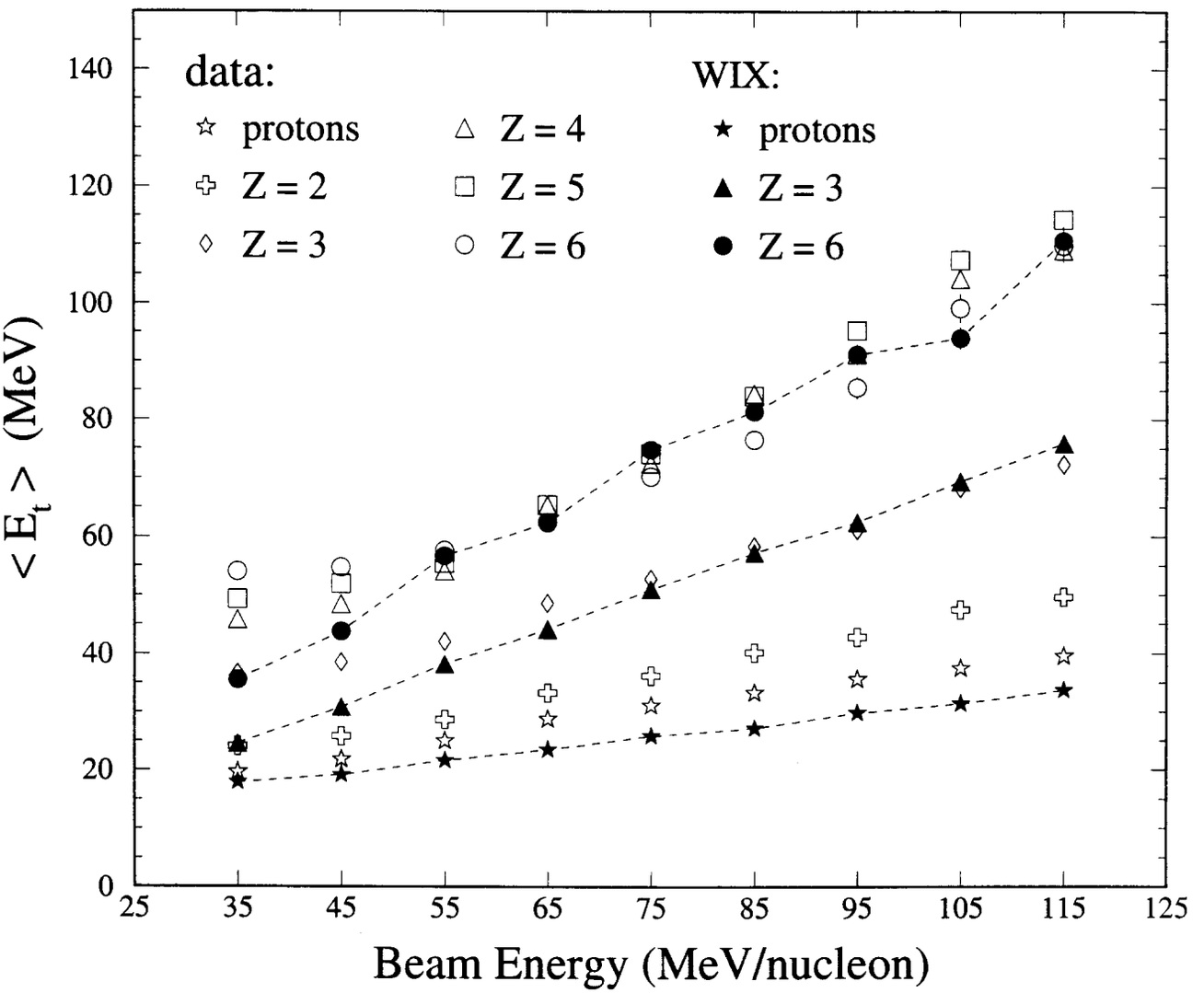
data:
protons
Z = 2
Z = 3
Z = 4
Z = 5
Z = 6
WIX:
protons
Z = 3
Z = 6
< E_t > (MeV)
Beam Energy (MeV/nucleon)
0
20
40
60
80
100
120
140
25
35
45
55
65
75
85
95
105
115
125

Figure 6:

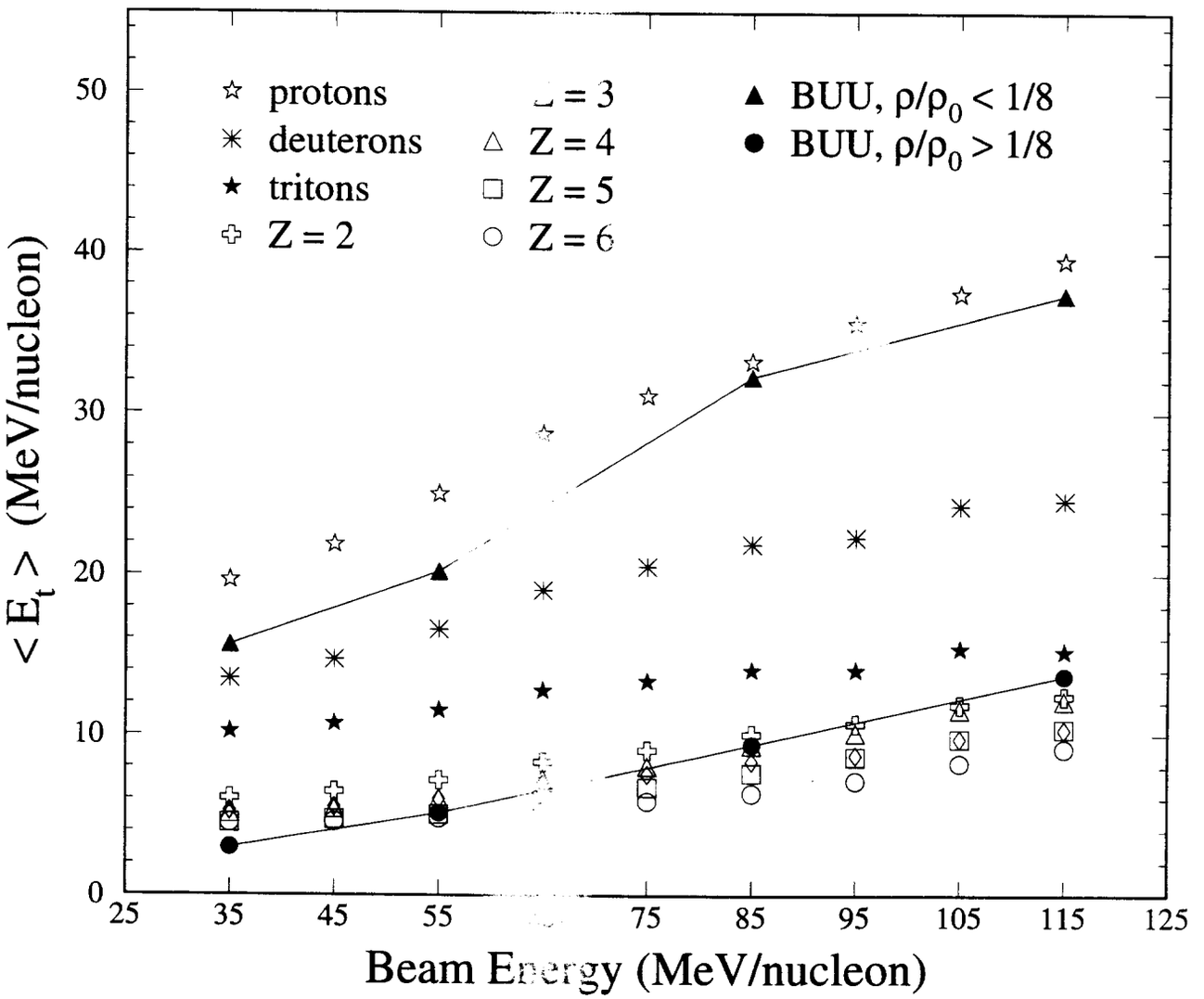
protons
deuterons
tritons
Z = 2
Z = 3
Z = 4
Z = 5
Z = 6
BUU, ρ/ρ0 < 1/8
BUU, ρ/ρ0 > 1/8
< Et > (MeV/nucleon)
Beam Energy (MeV/nucleon)
0
10
20
30
40
50
25
35
45
55
75
85
95
105
115
125

Figure 5:

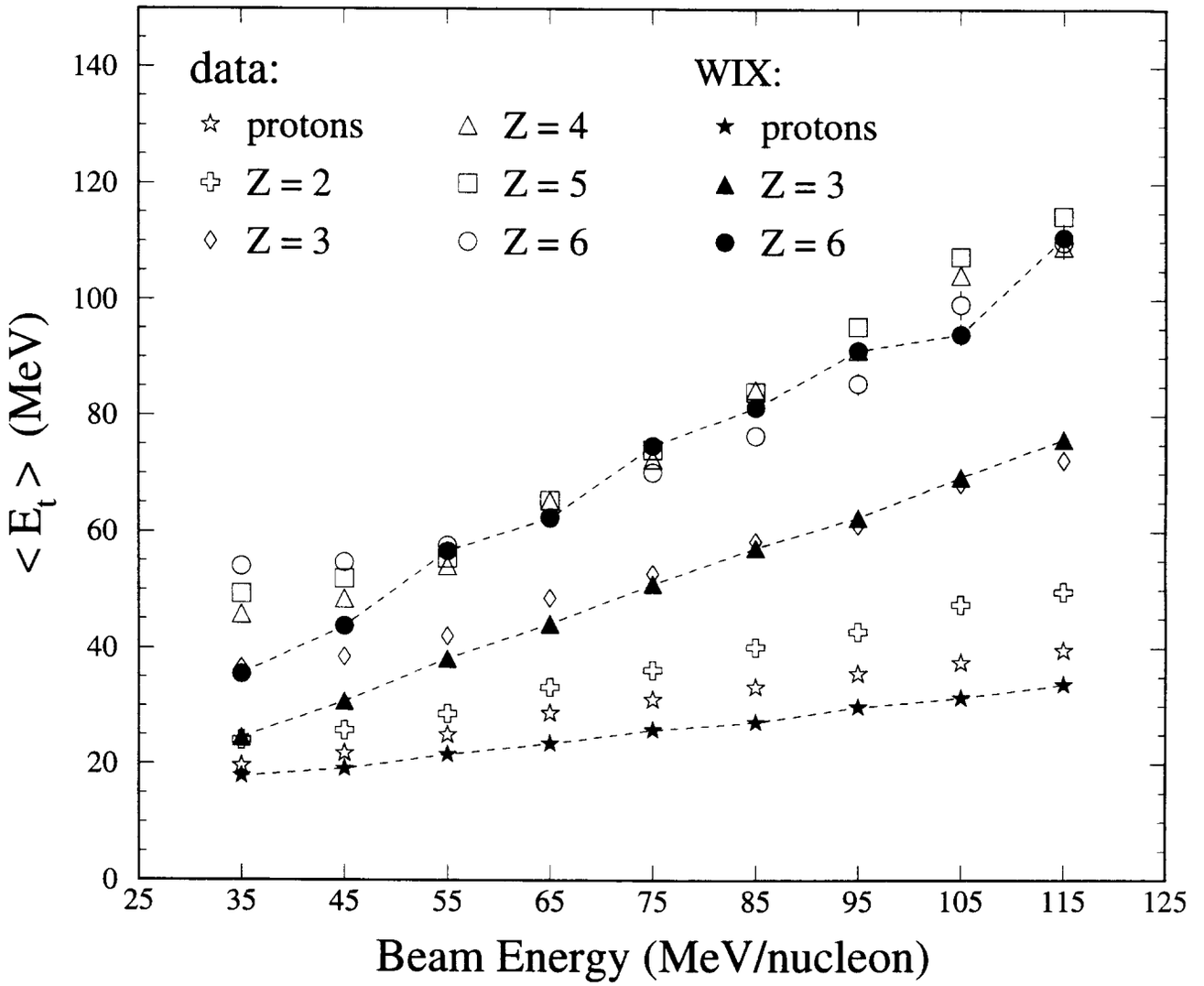
data:
protons
Z = 2
Z = 3
Z = 4
Z = 5
Z = 6
WIX:
protons
Z = 3
Z = 6
< E_t > (MeV)
Beam Energy (MeV/nucleon)
0
20
40
60
80
100
120
140
25
35
45
55
65
75
85
95
105
115
125

Figure 6: